Author Manuscript

Author Manuscript

Author Manuscript

Author Manuscript

HHS Public Access

Author manuscript

ACS Biomater Sci Eng. Author manuscript; available in PMC 2024 June 24.

Published in final edited form as:

ACS Biomater Sci Eng. 2024 May 13; 10(5): 2911–2924. doi:10.1021/acsbiomaterials.3c01704.

Modulating Lipid-Polymer Nanoparticles' Physicochemical Properties to Alter Macrophage Uptake

Elizabeth C. Bender,
Department of Biomedical Engineering, The University of Texas at Austin, Austin, Texas 78712, United States

Alisha J. Sircar,
Department of Biomedical Engineering, The University of Texas at Austin, Austin, Texas 78712, United States

Elle K. Taubenfeld,
Department of Biomedical Engineering, The University of Texas at Austin, Austin, Texas 78712, United States; Department of Molecular Biosciences, The University of Texas at Austin, Austin, Texas 78712, United States

Laura J. Suggs
Department of Biomedical Engineering, The University of Texas at Austin, Austin, Texas 78712, United States

Abstract

Macrophage uptake of nanoparticles is highly dependent on the physicochemical characteristics of those nanoparticles. Here, we have created a collection of lipid-polymer nanoparticles (LPNPs) varying in size, stiffness, and lipid makeup to determine the effects of these factors on uptake in murine bone marrow-derived macrophages. The LPNPs varied in diameter from 232 to 812 nm, in storage modulus from 21.2 to 287 kPa, and in phosphatidylserine content from 0 to 20%. Stiff, large nanoparticles with a coating containing phosphatidylserine were taken up by macrophages to a much higher degree than any other formulation (between 9.3× and 166× higher than other LPNPs). LPNPs with phosphatidylserine were taken up most by M2-polarized macrophages, while those without were taken up most by M1-polarized macrophages. Differences in total LPNP uptake were not dependent on endocytosis pathway(s) other than phagocytosis. This work acts as a basis for understanding how the interactions between nanoparticle physicochemical characteristics may act synergistically to facilitate particle uptake.

Corresponding Author: **Laura J. Suggs** – *Department of Biomedical Engineering, The University of Texas at Austin, Austin, Texas 78712, United States*; suggs@utexas.edu.

The authors declare no competing financial interest.

ASSOCIATED CONTENT

Supporting Information

The Supporting Information is available free of charge at https://pubs.acs.org/doi/10.1021/acsbiomaterials.3c01704.

Additional TEM images of PEGDA cores (Figure S1); coating all polymeric cores to produce 8 LPNPs (Figure S2); additional TEM images of large LPNPs (Figure S3); additional TEM images of small LPNPs (Figure S4); thin-layer chromatography controls (Figure S5); fluorescence of LPNPs in media (E_X: 585 nm, E_m: 635 nm) (Figure S6), and uptake is not dependent upon ζ-potential of final LPNP (Figure S7) (PDF)

Author Manuscript Author Manuscript Author Manuscript Author Manuscript

Graphical Abstract

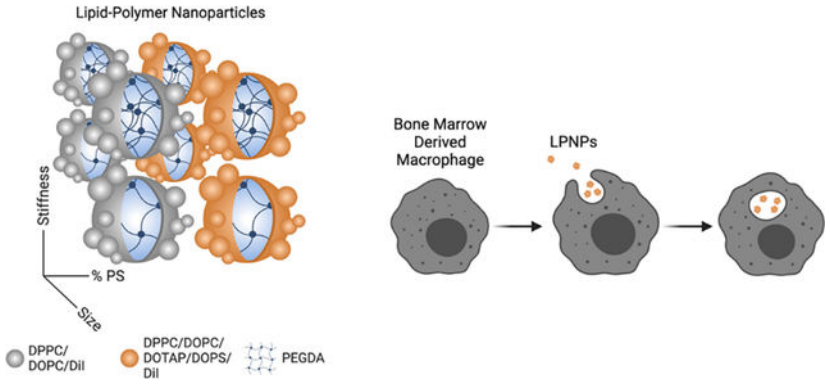

Keywords

macrophage; lipid-polymer nanoparticle; stiffness; size; phosphatidylserine; endocytosis

1. INTRODUCTION

Nanoparticles used as vehicles for drug delivery are a popular area of study due to their improved targeting of cells or tissues of interest, increased circulation times, and decreased off-target effects compared to drugs alone.[1–5] However, most of the first-generation nanoparticle carriers on the market were chosen because they are inert vessels for housing the drugs of interest.[6] Research is now being conducted on how active targeting strategies and the underlying physical characteristics of nanoparticles can play a role in their uptake by cells.[7,8] We are interested in how the nanoparticle physicochemical properties can be chosen to maximize uptake for future drug delivery applications.

A cell type that can be readily targeted with nanoparticles to ameliorate symptoms in a variety of conditions, like cancer and chronic inflammatory diseases, is the macrophage.[9,10] Macrophages are responsible for disease progression and severity in chronic autoimmune diseases like rheumatoid arthritis, systemic lupus erythematosus, and type 1 diabetes mellitus, so they are a good therapeutic target.[11–15] Macrophages also readily endocytose nano- and microparticles, making targeting them easier than many other cell types.

In a healthy individual, over one billion apoptotic cells are cleared every day by the immune system, primarily by macrophages and dendritic cells.[16] One way in which macrophages can target apoptotic cells is through “eat me” signals like phosphatidylserine (PS). PS is a phospholipid that is sequestered in the inner cell membrane leaflet in a living cell. When that cell undergoes apoptosis, the membrane loses its anisotropy, revealing PS on its surface. Macrophages have a variety of PS receptors on their surfaces that can bind with PS to clear apoptotic cells from circulation.[17] When macrophages endocytose cells after recognizing PS on their surface, they take on a more anti-inflammatory phenotype. This includes an increase in release of anti-inflammatory molecules like TGF-β and IL-10 and a decrease in production of pro-inflammatory molecules like TNF-α and IL-1β through activation of PPARγ and regulation of NF-κB.18 We can exploit the native clearance of apoptotic cells

Author Manuscript Author Manuscript Author Manuscript Author Manuscript

by adding PS to the surface of nanoparticles to target macrophages for the treatment of inflammatory conditions. This can act as both a targeting molecule and a primer for the anti-inflammatory cascade when paired with anti-inflammatory cargo.

Previously, we have designed an apoptotic body mimicking nanoparticle to reduce pro-inflammatory polarization of macrophages through presentation of PS-containing cell membranes on the surface of polymeric nanoparticles.[19,20] These nanoparticles reduced inflammation, but we are now interested in how their underlying physical characteristics could be tuned to further improve their uptake. These findings could be used in combination with anti-inflammatory drugs to provide the best treatment for chronic inflammatory conditions through targeted delivery to macrophages.

Nanoparticle properties can also affect macrophages' ability to endocytose nanoparticles through different pathways. Studies modulating one property at a time (i.e., surface coating, size, or stiffness) indicate that nanoparticles with PS,[21–24] stiffer nanoparticles,[25–29] and larger nanoparticles[30–32] tend to be taken up faster and to a higher degree than those without PS, those that are softer, and those that are smaller. However, the impact of the interactions among these characteristics on macrophage uptake has not been widely studied. The literature also shows that the pathway by which macrophages take up nanoparticles is dependent upon these characteristics. Endocytosis pathways have been determined to be size-,[33,34] stiffness-,[27,35] and ligand-dependent.[36,37] We aim to design an array of nanoparticles that can be tuned in these three dimensions while keeping other characteristics, such as ζ-potential, base material, and morphology consistent. In this study, we use a polymeric nanoparticle core that can be easily tuned in size and stiffness with a lipid coating that can mimic the surface of a living or apoptotic cell.

2. MATERIALS AND METHODS

2.1. Materials.

Cyclohexane, poly(ethylene glycol) diacrylate (M_W 700 Da) (PEGDA), 2-carboxyethyl acrylate (CEA), 2-hydroxy-2-methylpropiophenone (HMP), 1,1′-dioctadecyl-3,3,3′,3′-tetramethylindocarbocyanine perchlorate (DiI), fetal bovine serum, Span 80, Tween 80, cytochalasin D, 5-(*N*-ethyl-*N*-isopropyl)amiloride, and ES9–17 were purchased from Sigma-Aldrich. 1,2-Dipalmitoyl-*sn*-glycero-3-phosphocholine (DPPC), 1,2-dioleoyl-*sn*-glycero-3-phosphocholine (DOPC), 1,2-dioleoyl-3-trimethylammonium-propane (DOTAP), and 1,2-dioleoyl-*sn*-glycero-3-phospho-L-serine (DOPS) were purchased from Avanti Polar Lipids. Repligen Biotech CE Dialysis Membrane (MWCO 300 kDa) was purchased from Spectrum Chemical. Female FVBn mice were purchased from Charles River Laboratories. RPMI 1640 with L-glutamine was purchased from Caisson Laboratories. Penicillin-streptomycin was purchased from Thermo Fisher.

2.2. Cell Culture.

Bone marrow-derived macrophages (BMDMs) were isolated and cultured as previously described.[38] Briefly, the hindlimbs of a female FVBn mouse were extracted. Bone marrow was flushed out of the shafts of the bones using sterile phosphate-buffered saline (PBS). The

Author Manuscript Author Manuscript Author Manuscript Author Manuscript

cells were centrifuged, resuspended in media (RPMI 1640 medium + 10% heat-inactivated fetal bovine serum + 100 U/mL penicillin + 100 μg/mL streptomycin), and strained to remove any bone fragments. The cells were counted using a hemocytometer and adjusted to a concentration of 1 million cells/mL. Macrophage colony-stimulating factor (MCSF) was added to a final concentration of 10 ng/mL. Cells were plated and grown for 7 days with media changes on days 3, 5, and 7 to differentiate the cells to macrophages. Experiments were performed beginning on day 7.

2.3. Nanoparticle Core Synthesis.

Polymeric nanoparticle cores were synthesized through a water-in-oil emulsion templating technique modified from a previously described protocol.[25] Briefly, 1 mL of an aqueous phase of water, PEGDA, and CEA was added into 15 mL of cyclohexane with 300 mg of Span 80 and 100 mg of Tween 80 as emulsifiers while stirring. PEGDA was chosen as the main polymer due to its ability to cross-link via free radical polymerization and its wide range in elastic modulus. CEA was added to stabilize charge within the nanoparticles and improve precipitation into cold ethanol when necessary.[39] Soft nanoparticles were produced with 10% PEGDA and 1% CEA and stiff nanoparticles were produced with 40% PEGDA and 1% CEA. The emulsion was stirred for 5 min before being sonicated for 2 min to reduce the emulsion droplet size. If needed, multiple emulsions were pooled together into one round-bottom flask to increase the number of nanoparticles produced. HMP was added as a photoinitiator at a ratio of 5 μL/mL of emulsion. Oxygen was purged from the emulsion using nitrogen for 30 min then the emulsion was ultraviolet (UV) (λ = 365 nm) exposed for 15 min to cross-link the nanoparticles. The emulsion was stirred for an additional 1 h to ensure complete polymerization via free radical formation. The nanoparticles were washed 3× by mixing the emulsion with an equal volume of cold ethanol and centrifuging at 10,000*g* for 10 min at 8 °C. The final pellet was resuspended in water and dialyzed against water for 2 days to remove any excess ethanol, cyclohexane, or surfactants.

The resulting purified nanoparticles were separated based on size using differential centrifugation. Nanoparticles were centrifuged for 20 min at 1000*g*. The pellet was resuspended in water, and the supernatant was centrifuged at 5000*g*. This process of separating the pellet and supernatant and centrifuging the supernatant at a higher speed was repeated for 10,000, 15,000, and 20,000*g*. Each pellet was washed with water and centrifuged again at the same speed to remove any smaller nanoparticle contaminants.

2.4. Lipid-Polymer Nanoparticle Production.

Polymeric nanoparticle cores were coated in lipids using thin film hydration and sonication. Lipids dissolved in chloroform, either DPPC/DOPC/DiI 50/50/0.1 or DPPC/DOPC/DOTAP/DOPS/DiI 50/6-9/21-24/20/0.1, were dried into a thin film on a round-bottomed flask using a rotary evaporator. The amounts of DOTAP and DOPC were varied from batch to batch to produce a neutral liposome. The films were stored under a vacuum overnight to ensure complete removal of chloroform. The films were dissolved in water to 2 mg/mL at 55 °C for 30 min while rotating to form large multilamellar vesicles (LMVs). The LMVs were sonicated for 4 min at room temperature, rested for 2 min on ice, and then repeated for a total of 4 rounds to form small unilamellar vesicles (SUVs). The SUVs were centrifuged

Author Manuscript Author Manuscript Author Manuscript Author Manuscript

for 3 min at 10,000*g* to pellet and remove any titanium contamination from the sonic probe. Nanoparticle cores were coated by mixing with SUVs at a ratio of 1.25 mg lipid/7300 mm^2 total nanoparticle core surface area. This corresponds to 1.25 mg lipid/10^{11} smallest cores (St-S). The SUV/core mixtures were shaken at room temperature at 500 rpm overnight to facilitate coating. The coated nanoparticles were separated from excess SUVs by centrifuging at 20,000*g* for 20 min and washing 1× in water. The lipid-polymer nanoparticles (LPNPs) were then resuspended in water.

2.5. Nanoparticle Characterization.

The storage and loss moduli of the bulk PEGDA hydrogels were measured via rheometry. A mixture of 10 or 40% PEGDA, 1% CEA, and 1% HMP in water was added to a PDMS mold and UV-exposed for 30 min to cross-link the hydrogels. The hydrogels were hydrated in water overnight, cut into 8 mm × 1 mm cylinders, and measured on an Anton Paar Physica MCR 101 rheometer with a parallel plate geometry at 0.1% strain.

Nanoparticle size and ζ-potential were measured using a Malvern Zetasizer Nano ZS. *Z*-average diameter was reported for nanoparticle size. Size and ζ-potential measurements were run in triplicate. Nanoparticle concentration and scattered light intensity were measured by using Nanoparticle Tracking Analysis (NTA) on a Malvern NanoSight NS300. Five 20 s videos were analyzed for each sample to determine the concentration of nanoparticles. A separate set of five 20 s videos with the incident light intensity held constant were analyzed to measure the intensity of the light scattered by the nanoparticles to compare nanoparticle densities. Images of the nanoparticles were taken using an FEI Tecnai transmission electron microscope at 80 kV. Carbon-coated copper grids (Electron Microscopy Science) were plasma treated before the addition of the sample and then stained with 2% uranyl acetate.

2.6. Nanoparticle Uptake.

LPNPs were added to the BMDM culture at a surface area of 6500 mm^2/mL, which corresponds approximately to a maximum concentration of 4×10^{10} particles/mL for the smallest LPNP formulation (PS-St-S). Equivalent surface area was calculated using dynamic light scattering (DLS) *Z*-average diameter (d) and NTA concentration (LPNP Number/Volume) using the following equation

$$\frac{\text{surface area}}{\text{volume}} = \frac{\text{LPNP number}}{\text{volume}} \times \pi d^2 \quad (1)$$

After 4–24 h, the media was removed, and the cells were washed with PBS 2 times to remove unbound LPNPs before replacing with fresh media. The cells were imaged at 20× magnification with an Incucyte S3 Live Cell Analysis Instrument (Sartorius). The phase contrast and red fluorescent channels were used to measure the cells and LPNPs, respectively. Nine images/well with three wells/LPNP conditions were taken. The Incucyte software was used to measure cell confluence and fluorescence intensity within the cells

Author Manuscript Author Manuscript Author Manuscript Author Manuscript

from the phase contrast and red channels, respectively. For PS-St-L LPNPs measured over time, relative uptake compared to 0 h was calculated as follows

$$\text{uptake}_{\text{rel.}t0} = \frac{\frac{\text{integrated red intensity}}{\text{phase area}}}{\left(\frac{\text{integrated red intensity}}{\text{phase area}}\right)_{t0}} \tag{2}$$

For experiments with all 8 LPNPs at 12 h, baseline fluorescence of BMDMs without LPNPs was subtracted from all values. Total fluorescence of the LPNP-containing media was measured by using a BioTek Cytation 3 microplate reader. Relative uptake across LPNPs was calculated as follows

$$\text{uptake}_{\text{rel.LPNP}} = \frac{\frac{\text{integrated red intensity} \div \text{phase area}}{\text{total LPNP red intensity}}}{\left(\frac{\text{integrated red intensity} \div \text{phase area}}{\text{total LPNP red intensity}}\right)_{\text{maxLPNP}}} \tag{3}$$

2.7. Uptake by Polarized Macrophages.

BMDMs were polarized with 50 ng/mL LPS (M1) or 20 ng/mL IL-4 (M2) for 24 h. LPNPs were then added for 12 h before being washed with PBS and imaged using the Incucyte S3. Relative uptake across-polarizations within each LPNP was calculated as follows

$$\text{uptake}_{\text{rel.M0}} = \frac{\frac{\text{integrated red intensity}}{\text{phase area}}}{\left(\frac{\text{integrated red intensity}}{\text{phase area}}\right)_{\text{M0}}} \tag{4}$$

2.8. Endocytosis Inhibition.

Cytochalasin D (cytoD), 5-(*N*-ethyl-*N*-isopropyl)amiloride (EIPA), and ES9–17 were added to a BMDM culture for 30 min to inhibit different endocytosis pathways (Table 1). LPNPs were added to the culture at a surface area of 6500 mm^2/mL along with the inhibitors. After 12 h, the BMDMs were washed twice with PBS and imaged using the Incucyte S3. The cell confluence and red fluorescence intensity were measured on Incucyte software. Percent uptake with each inhibitor was found as follows

$$\text{percent uptake} = \frac{\left(\frac{\text{integrated red intensity}}{\text{phase area}}\right)_{\text{inhibitor}}}{\left(\frac{\text{integrated red intensity}}{\text{phase area}}\right)_{\text{no inhibitor}}} \times 100\% \tag{5}$$

Author Manuscript Author Manuscript Author Manuscript Author Manuscript

A decrease below 100% for an inhibitor and LPNP combination indicates use of that pathway in endocytosing the LPNP formulation. Results indicate the average of two experiments pooled together with three biological replicates per experiment.

2.9. Endocytosis Inhibition at Earlier Time Point.

BMDMs were plated on a 24-well glass-like polymer cell culture plate. After 7 days, BMDMs were pretreated with inhibitors for 30 min before adding LPNPs. After 4 h, inhibitors and LPNPs were removed, and cells were fixed with 4% formaldehyde for 15 min. The cells were stored in PBS under refrigeration and then imaged on a Nikon W1 spinning disk confocal microscope. Brightfield and red fluorescence images were taken at 20× magnification to visualize the cells and LPNPs, respectively. Ten images per well were taken. Fluorescence of LPNPs in each image was quantified using ImageJ. The background of each image was removed by auto thresholding using the triangle algorithm. The integrated intensity within each cell was measured using Analyze Particles and the integrated intensity was totaled for each image and then averaged across each well. Standard deviations are across technical replicates within one biological replicate.

2.10. Statistical Analysis.

Quantitative data is reported as mean ± standard deviation. Rheometry quantification was assessed with *t* tests, while the differences between all nanoparticles in other experiments were assessed with ANOVA. When appropriate, the ANOVA was followed by post hoc analysis using Tukey HSD. Reported significant results are at $p < 0.05$ unless otherwise noted. Statistical analysis was performed in R.

3. RESULTS AND DISCUSSION

3.1. Polymeric Nanoparticle Core Stiffness Is Modulated by Adjusting Polymer Fraction in Emulsion.

Nanoparticle cores were fabricated by using a water-in-oil emulsion technique, where the percent of PEGDA in the aqueous phase altered the stiffness of the nanoparticle (Figure 1A). An emulsion templating technique was chosen for its ability to vary the density of polymer within each nanoparticle while keeping the size fixed, based upon the initial emulsion droplet size. To understand how polymer density affects the stiffness of PEGDA-based hydrogels, we measured the moduli of macroscopic hydrogels with the same makeup as their nanoparticle counterparts. Storage and loss moduli of bulk PEGDA hydrogels were measured using a rheometer with a parallel plate geometry. Hydrogels with 10% PEGDA had storage and loss moduli of 21.2 and 1.62 kPa, respectively, while hydrogels with 40% PEGDA had storage and loss moduli of 287 and 49.5 kPa, respectively. This equates to the storage moduli of the 40% PEGDA hydrogels being 13.5 times higher than those made with 10% PEGDA (Figure 1B).

Direct measurements of nanoparticle stiffness using atomic force microscopy (AFM) were not performed due to the challenges and technical error associated with performing AFM on hydrogel nanoparticles.[40–42] However, nanoparticles made with 40% PEGDA scattered light at a significantly higher intensity than those made with 10% PEGDA,

Author Manuscript Author Manuscript Author Manuscript Author Manuscript

as measured using NTA, indicating a higher density of the polymer (Figure 1C). The refractive index of PEGDA hydrogels and therefore their ability to scatter light increases with increasing polymer concentration.[43] These results, along with qualitative differences seen in the transmission electron microscopy (TEM) images, provide confidence that the two nanoparticle stiffnesses chosen are significantly different from each other in the absence of a direct measure of nanoparticle stiffness. These formulations were labeled as “soft/So” and “stiff/St” for 10 and 40% PEGDA, respectively.

3.2. Differential Centrifugation Separates Polymeric Nanoparticle Cores by Size.

Despite the emulsion template providing consistency across stiffnesses, the nanoparticle cores within one batch were relatively polydisperse in size. To separate these nanoparticles into different size fractions, the nanoparticle cores were centrifuged at increasing speeds to pellet decreasing sized nanoparticles. Nanoparticle cores spun down at 5000*g* resulted in diameters of 517.9 and 443.6 nm for soft and stiff, while those spun down at 20,000*g* resulted in diameters of 206.8 and 152.1 nm for soft and stiff (Figure 2A and Table 2). The polydispersity index (PdI) for each nanoparticle core was low (0.203 or less), indicating monodisperse size fractions.[44] Soft nanoparticles spun down at 5000*g* were 2.5× larger in diameter than those spun down at 20,000*g* while stiff nanoparticles spun down at 5000*g* were 2.9× larger in diameter than those spun down at 20,000*g*. Nanoparticles in the 1000*g* fraction were discarded because of the high concentration of microscale aggregates, while those in the 10,000*g* and 15,000*g* fractions were of intermediate size and not used for any further experiments. Both the centrifugation speed and stiffness significantly impacted the resulting size of the nanoparticle cores. Each core composition is significantly different in size than all others; however, the impact of speed is much greater than that of stiffness. These nanoparticle core fractions were labeled as “large/L” and “small/S” for 5000*g* and 20,000*g* fractions, respectively. The ζ-potentials of all nanoparticle cores were between −35.6 and −39.5 mV, regardless of core stiffness or size (Figure 2B). Separation of nanoparticle cores by size was confirmed by TEM (Figures 2C and S1). Large differences in TEM size between soft and stiff cores are thought to be largely an artifact due to drying, exaggerating the small differences in diameter between stiffnesses measured using DLS.

3.3. Polymeric Nanoparticle Cores Are Coated in SUVs to Form LPNPs.

LPNPs were formed by producing SUVs with PS (“PS”: DPPC/DOPC/DOTAP/DOPS/DiI 50/6–9/21–24/20/0.1) and without PS (“PC”: DPPC/DOPC/DiI 50/50/0.1) and mixing with each nanoparticle core separately (Figure 3A). DOPC and DPPC were chosen as filler lipids due to their abundance in the cell membrane and their neutral charge. Unsaturated lipids (DOPC, DOPS, and DOTAP) were chosen for their fluidity and low elastic moduli, while saturated lipids (DPPC) were chosen to give the coatings structure. A ratio of 1:1 for unsaturated/saturated lipids was chosen empirically to balance the advantages of each. Since DOPS is negatively charged like the polymeric cores, SUVs made of DOPC + DPPC + DOPS did not coat the cores effectively, likely due to repulsive electrostatic forces. Positively charged DOTAP was added to neutralize the charge of the PS-containing SUV to provide a better coating and to mimic the ζ-potential of the PC SUVs. With the inclusion of both DOPS and DOTAP, small changes in the makeup of the PS SUVs would result in large shifts in ζ-potential from negative to positive charge. Obtaining a PS SUV with a ζ-potential

Author Manuscript Author Manuscript Author Manuscript Author Manuscript

as neutral as that of the PC SUV was not possible, explaining the small difference in ζ-potential between the two chosen SUVs. A slightly larger and variable percent of DOTAP (21–24%) compared to DOPS (20%) was used in the PS SUVs to produce SUVs with as neutral a charge as possible, which was not achieved with equal amounts of each. The amount of DOTAP added was adjusted due to batch variability in purchased stocks of lipids. DOPC was varied with DOTAP to keep the saturated:unsaturated lipid ratio consistent.

The PS and PC SUVs were 64.0 and 52.8 nm in diameter, respectively (Figures 3B and S2A). The ζ-potentials were 14.2 and 7.3 mV for PS and PC SUVs, respectively (Figures 3C and S2B). The small size of the SUVs imparted a drastic curvature of their surfaces, making them less stable and more likely to fuse and reform around the nanoparticle cores. An equivalent surface area of each nanoparticle core was coated in lipid to coat all cores as evenly as possible.

Coating the nanoparticle cores in SUVs resulted in an increase in the diameter of the nanoparticles and an increase in the ζ-potential toward the weakly positively charged ζ-potential of the SUVs, as is demonstrated with PS-St-L LPNPs (Figure 3B–C). The opposing charges of the cores and SUVs facilitated coating through electrostatic interactions. TEM images show that this coating was multilamellar and bleb-like at times, resembling a blebbing apoptotic body (Figure 3D).

For all formulations except PS-So-L, the final LPNPs were significantly larger in diameter and more positive in ζ-potential than their cores (Figure S2). Within the final collection of LPNPs, there were no differences within each size group, with PC-St-L being the only large LPNP not significantly larger than its small counterpart (Figure 4A and Table 3). Soft LPNPs tended to have a higher PdI than stiff LPNPs, indicating a wider range of diameters within each soft LPNP sample. The ζ-potentials of all LPNPs were close to neutral, ranging from −6.3 to 11.6 mV (Figure 4B). PS and stiff characteristics caused a slight increase in the ζ-potential over PC and soft characteristics. However, nanoparticles are considered neutral between −10 and +10 mV, which is approximately the range of the LPNPs.[45] The standard deviations of all LPNP ζ-potentials were large, indicating substantial batch-to-batch variation of LPNPs. Due to the consistency of the sizes and ζ-potentials of the cores and the SUVs, this variability comes from the coating process itself. We theorize that the differences in ζ-potential between PS-St and PS-So LPNPs are due to the arrangement of lipids within the coatings. In the PS-St LPNPs, the final ζ-potentials mimic those of SUVs used to coat the stiff cores. However, in the PS-So LPNPs, the final ζ-potentials are more neutral, indicating that more of the negatively charged DOPS is being presented on the surface of the LPNPs compared to positively charged DOTAP. This is either caused by or responsible for the aggregation/layering of lipid on the surface of the PS-So LPNPs, increasing their diameters slightly.

TEM images of each LPNP show the presence of lipid on the polymer core surfaces (Figures 4C and S3–S4). This lipid coating occasionally surrounded multiple cores into one large aggregate (PC-St-L) but was often one core surrounded by a multilamellar lipid structure created by the fusing of small SUVs together on the surface of the core. Aggregation and

Author Manuscript Author Manuscript Author Manuscript Author Manuscript

multilamellar coating account for the increase in size following coating seen in Figure 4A that is greater than the ~10 nm increase that would indicate coating in a single lipid bilayer.

Thin-layer chromatographs stained with ninhydrin for DOPS and sulfuric acid for DOPC, DOTAP, and DOPS show that the lipids contained in both SUVs were present on the surfaces of their corresponding final LPNPs (Figures 4D and S5). DiI is also visible in the ninhydrin-stained chromatograph, but this is due to the visible pink band of the DiI and not staining with ninhydrin. PC-coated LPNPs stain darker with sulfuric acid for DOPC, corresponding to the higher fraction of DOPC in their coating than the PS-coated LPNPs. The 8 LPNPs produced (Table 4) were then used to understand the impact of their physicochemical characteristics on uptake by macrophages.

3.4. LPNP Uptake Increases over Time while Cell Confluency Decreases.

BMDMs were plated in 96-well plates and differentiated for 7 days. To determine the ideal time point to compare uptake, PS-St-L LPNPs were given to BMDMs and uptake and cell confluence were measured at 4, 8, 12, and 24 h (Figure 5A). There was a steady decrease in the confluence of the BMDMs over time both with (PS-St-L) and without (control) the inclusion of LPNPs (Figure 5B). There was no significant difference in confluence between PS-St-L and control. Uptake of PS-St-L LPNPs relative to background fluorescence increases significantly over control fluorescence at 12 and 24 h (Figure 5C). This data was fit using the Boltzmann sigmoid function.

Final uptake experiments were conducted at 12 h because this time point balanced uptake and cell survival well in preliminary studies with only PS-St-L LPNPs. This time point is within the linear growth phase of uptake. At earlier time points (4 and 8 h), there was not yet substantial accumulation of any LPNPs within the macrophages. At later time points, all cells, including the nanoparticle-free control, began to die due to a lack of stimulation from MCSF while uptake also leveled off. At 12 h, there was a significant accumulation of LPNPs within cells but limited cell death compared to 24 h.

3.5. Unpolarized Macrophages Take Up LPNPs to Varying Degrees.

LPNPs were added to media at a surface area concentration of 6500 mm^2/mL. The cells were incubated with LPNPs for 12 h before removing the unbound LPNPs for imaging. After 12 h, PS-St-L LPNPs were taken up more than their soft (PS-So-L), small (PS-St-S), and PC (PC-St-L) counterparts (Figures 6 and S6). PS-So-L and PS-St-S were taken up more than their PC counterparts (PC-So-L and PC-St-S, respectively). By far, PS-St-L LPNPs were taken up the most, with all other LPNPs being taken up over 9.3× less.

PS, stiff, and large being the characteristic levels that increased uptake of LPNPs corresponds with findings from other groups throughout literature when these characteristics were tested individually.[21–32] When all three favorable characteristics were present (PS-St-L), there was the greatest uptake by a large margin. This is the only formulation that produced significantly higher uptake compared with other PS-coated LPNPs. Out of the three characteristics, PS was the only one that was necessary for any substantial uptake of LPNPs. PS acts as an active targeting molecule, binding to PS receptors on the surface of the macrophages. PC-coated LPNPs showed very little fluorescence within macrophages due to

Author Manuscript Author Manuscript Author Manuscript Author Manuscript

their lack of active targeting. When only PS plus one of the other favorable characteristics was present (PS-So-L and PS-St-S), there was significant uptake over those of some of the other LPNPs. No LPNPs with only one of the favorable characteristics exhibited significant uptake. However, the substantial gap between the uptake achieved by the PS-St-L LPNPs and the PS-So-L and PS-St-S LPNPs indicates that all three physicochemical characteristics are important in uptake and together they work synergistically to increase endocytosis.

Since nanoparticle ζ-potential is known to be important in how well nanoparticles are endocytosed,[46,47] we wanted to confirm that the differences in uptake between PC- and PS-coated LPNPs were due to the presence of PS and not the differences in ζ-potential. To accomplish this, we coated stiff large cores in different lipid coatings. These were PC and PS SUVs as before as well as SUVs made of DPPC/DOPC/DOTAP/DiI (50/48/2/0.1; “TAP”). The TAP SUVs were chosen to induce a positively charged surface onto the LPNPs such as the slightly more positive PS SUVs without the inclusion of PS as a targeting molecule. This decouples the impact of PS content from ζ-potential on the uptake of the LPNPs. Despite the PS-St-L LPNPs having a ζ-potential between the two other LPNPs, PS-St-L LPNPs were still taken up by BMDMs significantly more than the other LPNPs (Figure S7). This indicates that the positive charge associated with PS LPNPs does not account for the increased uptake over PC LPNPs. However, the PS-St-L LPNPs used in this experiment were more positively charged than usual due to a high ζ-potential in the coating SUV. This resulted in a lower relative uptake of PS-St-L LPNPs over PC-St-L LPNPs than was seen in other studies. This indicates that the ζ-potential does play a role in uptake in some way but is not relevant in the neutral (±10 mV) range that our standard LPNPs are within.

3.6. LPNP Uptake Is Dependent upon Macrophage Phenotype and Lipid Coating.

Due to the differences in uptake dependent upon lipid coating, polarized uptake was divided into two experiments, one with PS LPNPs and one with PC LPNPs. When compared to uptake by M0 macrophages, M2 macrophages took up more nanoparticles across all four PS LPNPs (Figure 7). This increase was more pronounced for the PS-So LPNPs. Compared to M0 macrophages, M1 macrophages tended to endocytose fewer PS LPNPs, although this decrease was not significant. This creates an overall uptake hierarchy of M2 > M0 ≥ M1 for PS LPNPs.

Results differed when testing the polarized uptake of PC LPNPs. When compared to uptake by M0 macrophages, M1 macrophages took up more nanoparticles across all four PC LPNPs (Figure 8). This was followed by M2 macrophages, with M0 macrophages taking up the fewest nanoparticles, resulting in an uptake hierarchy of M1 > M2 > M0 for PC LPNPs.

Macrophage polarization is known to impact how well nanoparticles are taken up. However, there is no clear consensus on what polarization causes the most endocytosis. In many nanoparticle systems, M2 macrophages take up more particles than M0 or M1 macrophages, which is the same as what we see in PS LPNP experiments.[48,49] However, in other studies, M1 macrophages have been seen to take up more nanoparticles, which is what we see in PC LPNP experiments.[50,51] These differences may be due to differences in both the macrophage sources and nanoparticle characteristics. For instance, M2 macrophages are upregulated in

Author Manuscript Author Manuscript Author Manuscript Author Manuscript

PS receptors like TIM-4 and stabilin-1.[52,53] Therefore, this increased preference for binding with PS may be the cause of the increased uptake of PS LPNPs.

The differences in polarized uptake between PS and PC LPNPs may be due to differences in specific vs nonspecific uptake as well as total uptake of each subset. We hypothesize that M1 macrophages take up more nanoparticles in a nonspecific manner than M2 or M0 cells. This accounts for the increase in the uptake of PC LPNPs by M1 macrophages. Since the total uptake of PC LPNPs is minimal compared to the total uptake of PS LPNPs, a similar increase in nonspecific uptake of PS LPNPs by M1 macrophages may be concealed. PS receptor-mediated endocytosis, which is upregulated in M2 macrophages, is a much stronger uptake mechanism than the upregulation of nonspecific uptake by M1 macrophages. The variations in nanoparticle surfaces lead to the differences seen in polarized uptake between PS and PC LPNPs.

3.7. Macrophages Use Multiple Endocytosis Pathways to Take Up PS LPNPS.

To inhibit endocytosis pathways individually, we chose three chemical inhibitors. There is no inhibitor specific for phagocytosis, so cytoD was used as a general inhibitor for all actin-dependent endocytosis. These pathways include phagocytosis, macropinocytosis, clathrin-mediated endocytosis, and caveolin-mediated endocytosis.[54,55] Caveolin-mediated endocytosis is size-limited, taking up nanoparticles ~60 nm in diameter, much smaller than any LPNPs tested here.[56] Therefore, it was not investigated in our studies. If the uptake of an LPNP condition was inhibited by cytoD but not by any other inhibitor, it would be assumed that the LPNPs were taken up by phagocytosis as the primary mechanism. Endocytosis pathways of PC LPNPs were not investigated due to the low total uptake of these nanoparticles.

Across all PS LPNPs, treatment with all inhibitors for 12 h resulted in a decrease in total LPNP uptake (Figure 9). Treatment with cytoD reduced the uptake to a negligible amount, indicating that LPNPs are taken up in an actin-dependent manner. This also confirms that LPNPs were actively endocytosed and not merely adsorbed onto the surface of the macrophages. Uptake of all LPNPs was also reduced when treated with EIPA, a macropinocytosis inhibitor, and ES9–17, a CME inhibitor. This suggests that all PS LPNPs are taken up to a significant extent by multiple pathways.

To confirm if decreases in uptake after inhibiting actin polymerization, sodium-proton exchange, and clathrin heavy chain for 12 h was due to inhibition of specific uptake pathways or a reduction of receptors on the cell surface through inhibited cell membrane recycling, we treated BMDMs with chemical endocytosis inhibitors and LPNPs for 4 h then imaged using confocal microscopy. Increased resolution in the confocal images and more control over fluorescence wavelength compared to the Incucyte images allowed us to see accumulation of the LPNPs within the cells at this earlier time point when they were not visible using the Incucyte. At 4 h, cytoD significantly inhibited uptake of all LPNPs (Figure 10). However, ES9–17 had no effect, and EIPA only reduced uptake in PS-St-S LPNPs, despite the widespread effects both inhibitors had at 12 h. Decrease in cytoD without decrease in another main pathway indicates that phagocytosis may be the main form of uptake of LPNPs at 4 h.

Author Manuscript Author Manuscript Author Manuscript Author Manuscript

The difference in uptake mechanism present at the different time points leads to two theories: (1) There are rate differences in each pathway leading to CME and macropinocytosis only being significantly used for LPNP uptake at longer time scales. Other groups have found that nanoparticle physicochemical characteristics both impact total cellular uptake as well as rate of uptake.[25,27,30,35,57] This could be due to saturation of cells with nanoparticles reducing further uptake or speed of different endocytosis pathways used. (2) Incubation of BMDMs with endocytosis inhibitors for 12 h leads to nonspecificity of the inhibitors. Nonspecificity could be a result of inhibition of membrane recycling of PS receptors, which would impact all receptor-mediated endocytosis, not just a single pathway.

CME is typically thought to only endocytose particles up to 150 nm.[58,59] This size is smaller than those of all LPNPs produced. Our results suggest that all PS LPNPs were taken up to some extent by CME at 12 h, regardless of size, which ranges from 232 to 812 nm in diameter. Other groups have made conclusions that nanoparticles greater than 150 nm can be taken up by CME, calling into question the traditional view on size restrictions of this pathway.[60] However, there is little evidence in the literature for nanoparticles >500 nm being taken up by CME. There are a few reasons we may see this in our system that do not compete with the current knowledge of CME size restrictions. One possibility is that BMDMs are only endocytosing small pieces of the DiI-labeled lipid coating and not the entire LPNP. BMDMs could be pulling vesicles off the surface of the LPNPs and internalizing them while leaving the PEGDA cores behind. A second possibility is that at 12 h, ES9–17 is inhibiting other forms of endocytosis like phagocytosis. ES9–17 blocks clathrin heavy chain, the main component that makes up clathrin-coated pits. However, clathrin heavy chain is also involved in the membrane recycling process.[61] It is possible that at 12 h, many PS receptors have been pulled off the cell surface but were not able to be put back on, reducing all receptor-mediated endocytosis.

The overall lack of substantial differences seen between PS-St-L and other PS LPNP endocytosis routes leads us to theorize that the elevated uptake of PS-St-L is due to improved phagocytosis and not differences in uptake through the other endocytosis pathways tested.

4. CONCLUSIONS

The experiments performed in this paper confirm that the interactions between physicochemical characteristics of nanoparticles are just as important as the characteristics themselves in cell-nanoparticle interactions. We found that the interaction between size, stiffness, and lipid makeup is integral with how macrophages take up those nanoparticles; however, the interactions between other characteristics like shape, surface roughness, and hydrophobicity were not investigated. Future studies will need to be performed to expand our knowledge on the interaction effects of other nanoparticle properties on uptake by macrophages and other cell types.

PS-St-L LPNPs can be used alone as a method for reprogramming of macrophages due to the anti-inflammatory effects of PS, or they can be used as base nanoparticles for the

Author Manuscript Author Manuscript Author Manuscript Author Manuscript

delivery of anti-inflammatory agents like TNFα siRNA, curcumin, or IL-10 plasmid.[62–64] These physicochemical characteristics can provide the best delivery of these anti-inflammatory agents to macrophages to allow for an optimal dose response and decreased off-target effects. By targeting and repolarizing macrophages, the cycle of inflammation in chronic inflammatory and autoimmune diseases can be disrupted to reduce symptoms and pause disease progression.

In this study, we created an array of eight lipid-polymer nanoparticles that are small/large, soft/stiff, and with/without PS. These LPNPs consist of a polymer core to impart physical attributes surrounded by a lipid coating to aid in cellular interactions. When given to bone marrow-derived macrophages, LPNPs that were large, stiff, and contained PS were taken up significantly more than any other formulation, demonstrating the importance of all three physicochemical characteristics on endocytosis and indicating that these characteristics work better together than alone. We also found that macrophage polarization drastically impacts the uptake of nanoparticles, with PS LPNPs taken up most by M2 macrophages and PC LPNPs taken up most by M1 macrophages. The endocytosis pathways used by macrophages to take up the PS LPNPs did not differ significantly across the LPNP formulations, despite differences in total uptake.

Supplementary Material

Refer to Web version on PubMed Central for supplementary material.

ACKNOWLEDGMENTS

The authors thank Chelsea Kraynak and Jessica Widman for helpful discussions regarding experimental design and the Brock lab for their assistance using the Incucyte. TEM was performed at the Center for Biomedical Research Support Microscopy and Imaging Facility at UT Austin (RRID# SCR_021756). The graphical abstract and Figures 1A and 3A were created with Biorender.com.

Funding

This work was funded by the National Institutes of Health (Grant #R56EB032211). Elizabeth Bender acknowledges the support of the University Graduate Continuing Fellowship from The University of Texas at Austin.

REFERENCES

(1). Couvreur P Nanoparticles in Drug Delivery: Past, Present and Future. Adv. Drug Delivery Rev. 2013, 65 (1), 21–23.

(2). Large DE; Abdelmessih RG; Fink EA; Auguste DT Liposome Composition in Drug Delivery Design, Synthesis, Characterization, and Clinical Application. Adv. Drug Delivery Rev 2021, 176, No. 113851.

(3). Yaghmur A; Mu H Recent Advances in Drug Delivery Applications of Cubosomes, Hexosomes, and Solid Lipid Nanoparticles. Acta Pharm. Sin. B 2021, 11 (4), 871–885. [PubMed: 33996404]

(4). Chandrakala V; Aruna V; Angajala G Review on Metal Nanoparticles as Nanocarriers: Current Challenges and Perspectives in Drug Delivery Systems. Emergent Mater. 2022, 5 (6), 1593–1615. [PubMed: 35005431]

(5). Gagliardi A; Giuliano E; Venkateswararao E; Fresta M; Bulotta S; Awasthi V; Cosco D Biodegradable Polymeric Nanoparticles for Drug Delivery to Solid Tumors. Front. Pharmacol. 2021, 12, No. 601626.

(6). Anselmo AC; Mitragotri S Nanoparticles in the Clinic: An Update. Bioeng. Transl. Med. 2019, 4 (3), No. e10143. [PubMed: 31572799]

Author Manuscript Author Manuscript Author Manuscript Author Manuscript

(7). Mitchell MJ; Billingsley MM; Haley RM; Wechsler ME; Peppas NA; Langer R Engineering Precision Nanoparticles for Drug Delivery. Nat. Rev. Drug Discovery 2021, 20 (2), 101–124. [PubMed: 33277608]

(8). Yusuf A; Almotairy ARZ; Henidi H; Alshehri OY; Aldughaim MS Nanoparticles as Drug Delivery Systems: A Review of the Implication of Nanoparticles' Physicochemical Properties on Responses in Biological Systems. Polymers 2023, 15 (7), No. 1596. [PubMed: 37050210]

(9). Hu G; Guo M; Xu J; Wu F; Fan J; Huang Q; Yang G; Lv Z; Wang X; Jin Y Nanoparticles Targeting Macrophages as Potential Clinical Therapeutic Agents Against Cancer and Inflammation. Front. Immunol. 2019, 10, No. 1998, DOI: 10.3389/fimmu.2019.01998.

(10). Bender EC; Kraynak C; Huang W; Suggs LJ Cell-Inspired Biomaterials for Modulating Inflammation. Tissue Eng., Part B 2022, 28, 279–294.

(11). Shapouri-Moghaddam A; Mohammadian S; Vazini H; Taghadosi M; Esmaeili S-A; Mardani F; Seifi B; Mohammadi A; Afshari JT; Sahebkar A Macrophage Plasticity, Polarization, and Function in Health and Disease. J. Cell. Physiol. 2018, 233 (9), 6425–6440.

(12). Yang X; Chang Y; Wei W Emerging Role of Targeting Macrophages in Rheumatoid Arthritis: Focus on Polarization, Metabolism and Apoptosis. Cell Proliferation 2020, 53 (7), No. e12854. [PubMed: 32530555]

(13). Ma W-T; Gao F; Gu K; Chen D-K The Role of Monocytes and Macrophages in Autoimmune Diseases: A Comprehensive Review. Front. Immunol. 2019, 10, No. 1140, DOI: 10.3389/fimmu.2019.01140.

(14). Espinoza-Jiménez A; Peón AN; Terrazas LI Alternatively Activated Macrophages in Types 1 and 2 Diabetes. Mediators Inflammation 2012, 2012, No. 815953.

(15). Udalova IA; Mantovani A; Feldmann M Macrophage Heterogeneity in the Context of Rheumatoid Arthritis. Nat. Rev. Rheumatol. 2016, 12 (8), 472–485. [PubMed: 27383913]

(16). Peng Y; Martin DA; Kenkel J; Zhang K; Ogden CA; Elkon KB Innate and Adaptive Immune Response to Apoptotic Cells. J. Autoimmun. 2007, 29 (4), 303–309. [PubMed: 17888627]

(17). Fadok VA; de Cathelineau A; Daleke DL; Henson PM; Bratton DL Loss of Phospholipid Asymmetry and Surface Exposure of Phosphatidylserine Is Required for Phagocytosis of Apoptotic Cells by Macrophages and Fibroblasts. J. Biol. Chem. 2001, 276 (2), 1071–1077. [PubMed: 10986279]

(18). Elliott MR; Koster KM; Murphy PS Efferocytosis Signaling in the Regulation of Macrophage Inflammatory Responses. J. Immunol. 2017, 198 (4), 1387–1394. [PubMed: 28167649]

(19). Kraynak CA; Yan DJ; Suggs LJ Modulating Inflammatory Macrophages with an Apoptotic Body-Inspired Nanoparticle. Acta Biomater. 2020, 108, 250–260. [PubMed: 32251779]

(20). Kraynak CA; Huang W; Bender EC; Wang J-L; Hanafy MS; Cui Z; Suggs LJ Apoptotic Body-Inspired Nanoparticles Target Macrophages at Sites of Inflammation to Support an Anti-Inflammatory Phenotype Shift. Int. J. Pharm. 2022, 618, No. 121634.

(21). Hosain MZ; Yuzuriha K; Khadijah; Takeo M; Kishimura A; Murakami Y; Mori T; Katayama Y Synergic Modulation of the Inflammatory State of Macrophages Utilizing Anti-Oxidant and Phosphatidylserine-Containing Polymer–Lipid Hybrid Nanoparticles. MedChemComm 2017, 8 (7), 1514–1520. [PubMed: 30108863]

(22). Shah NK; Gupta SK; Wang Z; Meenach SA Enhancement of Macrophage Uptake via Phosphatidylserine-Coated Acetalated Dextran Nanoparticles. J. Drug Delivery Sci. Technol. 2019, 50, 57–65.

(23). Gomi M; Sakurai Y; Sato M; Tanaka H; Miyatake Y; Fujiwara K; Watanabe M; Shuto S; Nakai Y; Tange K; Hatakeyama H; Akita H Delivering mRNA to Secondary Lymphoid Tissues by Phosphatidylserine-Loaded Lipid Nanoparticles. Adv. Healthcare Mater. 2023, 12 (9), No. 2202528.

(24). Brinkhuizen C; Shapman D; Lebon A; Bénard M; Tardivel M; Dubuquoy L; Galas L; Carpentier R Dipalmitoyl-Phosphatidylserine-Filled Cationic Maltodextrin Nanoparticles Exhibit Enhanced Efficacy for Cell Entry and Intracellular Protein Delivery in Phagocytic THP-1 Cells. Biomol. Concepts 2023, 14 (1), No. 20220029, DOI: 10.1515/bmc-2022-0029.

Author Manuscript Author Manuscript Author Manuscript Author Manuscript

(25). Anselmo AC; Zhang M; Kumar S; Vogus DR; Menegatti S; Helgeson ME; Mitragotri S Elasticity of Nanoparticles Influences Their Blood Circulation, Phagocytosis, Endocytosis, and Targeting. ACS Nano 2015, 9 (3), 3169–3177. [PubMed: 25715979]

(26). Tengjisi; Hui Y; Fan Y; Zou D; Talbo GH; Yang G; Zhao C-X Influence of Nanoparticle Mechanical Property on Protein Corona Formation. J. Colloid Interface Sci. 2022, 606, 1737–1744. [PubMed: 34507167]

(27). Hui Y; Yi X; Wibowo D; Yang G; Middelberg APJ; Gao H; Zhao C-X Nanoparticle Elasticity Regulates Phagocytosis and Cancer Cell Uptake. Sci. Adv. 2020, 6 (16), No. eaaz4316. [PubMed: 32426455]

(28). Zhang G; Xue H; Sun D; Yang S; Tu M; Zeng R Soft Apoptotic-Cell-Inspired Nanoparticles Persistently Bind to Macrophage Membranes and Promote Anti-Inflammatory and pro-Healing Effects. Acta Biomater. 2021, 131, 452–463. [PubMed: 34245890]

(29). Yildirim M; Weiss A-V; Schneider M The Effect of Elasticity of Gelatin Nanoparticles on the Interaction with Macrophages. Pharmaceutics 2023, 15 (1), No. 199. [PubMed: 36678828]

(30). Yu SS; Lau CM; Thomas SN; Jerome WG; Maron DJ; Dickerson JH; Hubbell JA; Giorgio TD Size- and Charge-Dependent Non-Specific Uptake of PEGylated Nanoparticles by Macrophages. Int. J. Nanomed. 2012, 7, 799–813.

(31). Walkey CD; Olsen JB; Guo H; Emili A; Chan WCW Nanoparticle Size and Surface Chemistry Determine Serum Protein Adsorption and Macrophage Uptake. J. Am. Chem. Soc. 2012, 134 (4), 2139–2147. [PubMed: 22191645]

(32). He C; Hu Y; Yin L; Tang C; Yin C Effects of Particle Size and Surface Charge on Cellular Uptake and Biodistribution of Polymeric Nanoparticles. Biomaterials 2010, 31 (13), 3657–3666. [PubMed: 20138662]

(33). Brown TD; Habibi N; Wu D; Lahann J; Mitragotri S Effect of Nanoparticle Composition, Size, Shape, and Stiffness on Penetration Across the Blood–Brain Barrier. ACS Biomater. Sci. Eng. 2020, 6 (9), 4916–4928. [PubMed: 33455287]

(34). Rejman J; Oberle V; Zuhorn IS; Hoekstra D Size-Dependent Internalization of Particles via the Pathways of Clathrin- and Caveolae-Mediated Endocytosis. Biochem. J. 2004, 377 (Pt 1), 159–169. [PubMed: 14505488]

(35). Banquy X; Suarez F; Argaw A; Rabanel J-M; Grutter P; Bouchard J-F; Hildgen P; Giasson S Effect of Mechanical Properties of Hydrogel Nanoparticles on Macrophage Cell Uptake. Soft Matter 2009, 5 (20), 3984–3991.

(36). Hauser D; Estermann M; Milosevic A; Steinmetz L; Vanhecke D; Septiadi D; Drasler B; Petri-Fink A; Ball V; Rothen-Rutishauser B Polydopamine/Transferrin Hybrid Nanoparticles for Targeted Cell-Killing. Nanomaterials 2018, 8 (12), No. 1065. [PubMed: 30562983]

(37). Chatterjee M; Ben-Josef E; Robb R; Vedaie M; Seum S; Thirumoorthy K; Palanichamy K; Harbrecht M; Chakravarti A; Williams TM Caveolae-Mediated Endocytosis Is Critical for Albumin Cellular Uptake and Response to Albumin-Bound Chemotherapy. Cancer Res. 2017, 77 (21), 5925–5937. [PubMed: 28923854]

(38). Rybalko V; Hsieh PL; Ricles LM; Chung E; Farrar RP; Suggs LJ Therapeutic Potential of Adipose-Derived Stem Cells and Macrophages for Ischemic Skeletal Muscle Repair. Regener. Med. 2017, 12 (2), 153–167.

(39). Stillman ZS; Jarai BM; Raman N; Patel P; Fromen CA Degradation Profiles of Poly(Ethylene Glycol) Diacrylate (PEGDA)-Based Hydrogel Nanoparticles. Polym. Chem 2020, 11 (2), 568–580. [PubMed: 33224282]

(40). Guo D; Xie G; Luo J Mechanical Properties of Nanoparticles: Basics and Applications. J. Phys. Appl. Phys. 2014, 47 (1), No. 013001.

(41). Eid J; Greige-Gerges H; Monticelli L; Jraij A Elastic Moduli of Lipid Membranes: Reproducibility of AFM Measures. Chem. Phys. Lipids 2021, 234, No. 105011.

(42). Paik P; Kar K; Deva D; Sharma A Measurement of Mechanical Properties of Polymer Nanospheres by Atomic Force Microscopy: Effects of Particle Size. Micro Nano Lett. 2007, 2, 72–77.

(43). Torres-Mapa ML; Singh M; Simon O; Mapa JL; Machida M; Günther A; Roth B; Heinemann D; Terakawa M; Heisterkamp A Fabrication of a Monolithic Lab-on-a-Chip Platform with

Author Manuscript Author Manuscript Author Manuscript Author Manuscript

Integrated Hydrogel Waveguides for Chemical Sensing. Sensors 2019, 19 (19), No. 4333. [PubMed: 31597248]

(44). Danaei M; Dehghankhold M; Ataei S; Davarani FH; Javanmard R; Dokhani A; Khorasani S; Mozafari MR Impact of Particle Size and Polydispersity Index on the Clinical Applications of Lipidic Nanocarrier Systems. Pharmaceutics 2018, 10 (2), No. 57. [PubMed: 29783687]

(45). Clogston JD; Patri AKζ-Potential Measurement. In Methods in Molecular Biology; Springer, 2011; Vol. 697, pp 63–70.

(46). Jeon S; Clavadetscher J; Lee D-K; Chankeshwara SV; Bradley M; Cho W-S Surface Charge-Dependent Cellular Uptake of Polystyrene Nanoparticles. Nanomaterials 2018, 8 (12), No. 1028. [PubMed: 30544753]

(47). Patil S; Sandberg A; Heckert E; Self W; Seal S Protein Adsorption and Cellular Uptake of Cerium Oxide Nanoparticles as a Function of ζ-potential. Biomaterials 2007, 28 (31), 4600–4607. [PubMed: 17675227]

(48). MacParland SA; Tsoi KM; Ouyang B; Ma X-Z; Manuel J; Fawaz A; Ostrowski MA; Alman BA; Zilman A; Chan WCW; McGilvray ID Phenotype Determines Nanoparticle Uptake by Human Macrophages from Liver and Blood. ACS Nano 2017, 11 (3), 2428–2443. [PubMed: 28040885]

(49). Hoppstädter J; Seif M; Dembek A; Cavelius C; Huwer H; Kraegeloh A; Kiemer AK M2 Polarization Enhances Silica Nanoparticle Uptake by Macrophages. Front. Pharmacol. 2015, 6, No. 129823, DOI: 10.3389/fphar.2015.00055.

(50). Herd HL; Bartlett KT; Gustafson JA; McGill LD; Ghandehari H Macrophage Silica Nanoparticle Response Is Phenotypically Dependent. Biomaterials 2015, 53, 574–582. [PubMed: 25890753]

(51). Qie Y; Yuan H; von Roemeling CA; Chen Y; Liu X; Shih KD; Knight JA; Tun HW; Wharen RE; Jiang W; Kim BYS Surface Modification of Nanoparticles Enables Selective Evasion of Phagocytic Clearance by Distinct Macrophage Phenotypes. Sci. Rep. 2016, 6, No. 26269.

(52). Kzhyshkowska J; Mamidi S; Gratchev A; Kremmer E; Schmuttermaier C; Krusell L; Haus G; Utikal J; Schledzewski K; Scholtze J; Goerdt S Novel Stabilin-1 Interacting Chitinase-like Protein (SI-CLP) Is up-Regulated in Alternatively Activated Macrophages and Secreted via Lysosomal Pathway. Blood 2006, 107 (8), 3221–3228. [PubMed: 16357325]

(53). Thornley TB; Fang Z; Balasubramanian S; Larocca RA; Gong W; Gupta S; Csizmadia E; Degauque N; Kim BS; Koulmanda M; Kuchroo VK; Strom TB Fragile TIM-4–Expressing Tissue Resident Macrophages Are Migratory and Immunoregulatory. J. Clin. Invest. 2014, 124 (8), 3443–3454. [PubMed: 24983317]

(54). Mooren OL; Galletta BJ; Cooper JA Roles for Actin Assembly in Endocytosis. Annu. Rev. Biochem. 2012, 81 (1), 661–686. [PubMed: 22663081]

(55). Lamaze C; Fujimoto LM; Yin HL; Schmid SL The Actin Cytoskeleton Is Required for Receptor-Mediated Endocytosis in Mammalian Cells*. J. Biol. Chem. 1997, 272 (33), 20332–20335. [PubMed: 9252336]

(56). de Almeida MS; Susnik E; Drasler B; Taladriz-Blanco P; Petri-Fink A; Rothen-Rutishauser B Understanding Nanoparticle Endocytosis to Improve Targeting Strategies in Nanomedicine. Chem. Soc. Rev. 2021, 50 (9), 5397–5434. [PubMed: 33666625]

(57). Gurnani P; Sanchez-Cano C; Xandri-Monje H; Zhang J; Ellacott SH; Mansfield EDH; Hartlieb M; Dallmann R; Perrier S Probing the Effect of Rigidity on the Cellular Uptake of Core-Shell Nanoparticles: Stiffness Effects Are Size Dependent. Small 2022, 18 (38), No. 2203070.

(58). Manzanares D; Ceña V Endocytosis: The Nanoparticle and Submicron Nanocompounds Gateway into the Cell. Pharmaceutics 2020, 12 (4), No. 371. [PubMed: 32316537]

(59). Rennick JJ; Johnston APR; Parton RG Key Principles and Methods for Studying the Endocytosis of Biological and Nanoparticle Therapeutics. Nat. Nanotechnol. 2021, 16 (3), 266–276. [PubMed: 33712737]

(60). Wolfram J; Nizzero S; Liu H; Li F; Zhang G; Li Z; Shen H; Blanco E; Ferrari M A Chloroquine-Induced Macrophage-Preconditioning Strategy for Improved Nanodelivery. Sci. Rep. 2017, 7 (1), No. 13738. [PubMed: 29062065]

(61). Stoorvogel W; Oorschot V; Geuze H A Novel Class of Clathrin-Coated Vesicles Budding from Endosomes. J. Cell Biol. 1996, 132 (1), 21–33. [PubMed: 8567724]

Author Manuscript Author Manuscript Author Manuscript Author Manuscript

(62). Jansen MAA; Klausen LH; Thanki K; Lyngsø J; Pedersen JS; Franzyk H; Nielsen HM; van Eden W; Dong M; Broere F; Foged C; Zeng X Lipidoid-Polymer Hybrid Nanoparticles Loaded with TNF siRNA Suppress Inflammation after Intra-Articular Administration in a Murine Experimental Arthritis Model. Eur. J. Pharm. Biopharm. 2019, 142, 38–48. [PubMed: 31199978]

(63). Wang J; Kang Y-X; Pan W; Lei W; Feng B; Wang X-J Enhancement of Anti-Inflammatory Activity of Curcumin Using Phosphatidylserine-Containing Nanoparticles in Cultured Macrophages. Int. J. Mol. Sci. 2016, 17 (6), No. 969. [PubMed: 27331813]

(64). Jain S; Tran T-H; Amiji M Macrophage Repolarization with Targeted Alginate Nanoparticles Containing IL-10 Plasmid DNA for the Treatment of Experimental Arthritis. Biomaterials 2015, 61, 162–177. [PubMed: 26004232]

Author Manuscript Author Manuscript Author Manuscript Author Manuscript

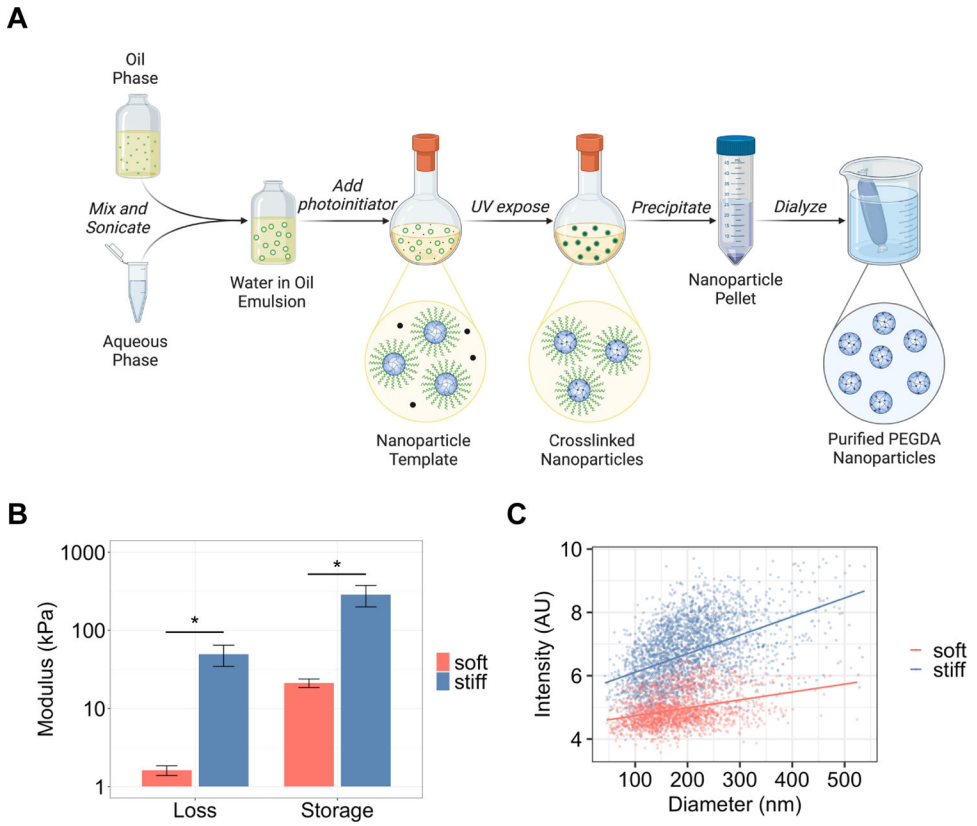

Figure 1.

Producing polymeric nanoparticle cores with a tunable stiffness. (A) Schematic of water-in-oil emulsion templating technique. An aqueous phase with various amounts of PEGDA is emulsified into an oil phase with a photoinitiator before being cross-linked under UV. Adjusting the amount of PEGDA in the aqueous phase allows for soft (10% PEGDA) or stiff (40% PEGDA) nanoparticles to be formed. (B) Macroscopic hydrogels of the same composition as soft and stiff nanoparticles show an increase in storage and loss moduli from 21.2 and 1.62 kPa for soft to 287 and 49.5 kPa for stiff ($n = 6$). (C) Nanoparticles with higher stiffness scatter light at a higher intensity across diameters using NTA. (*$p < 0.01$, t test).

Author Manuscript Author Manuscript Author Manuscript Author Manuscript

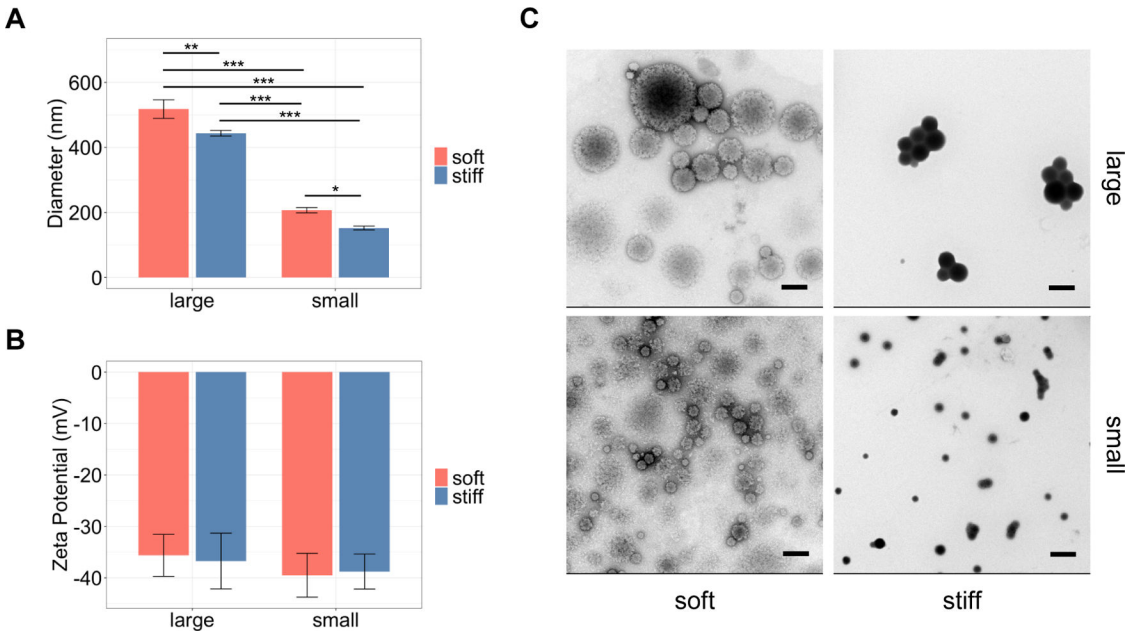

Figure 2.

Characterization of polymeric nanoparticle cores. (A) DLS *Z*-average shows that nanoparticle cores are separated into small and large fractions, with small differences in size between stiffnesses. (B) ζ-potentials are highly negative and consistent across all nanoparticle cores. (C) Representative TEM images confirm that nanoparticles in small and large fractions are different in size. Additional images can be found in Figure S1. Scale bar = 500 nm ($n = 5$, $^{*}p < 10^{-3}$, $^{**}p < 10^{-5}$, $^{***}p < 10^{-12}$, two-way ANOVA).

Author Manuscript Author Manuscript Author Manuscript Author Manuscript

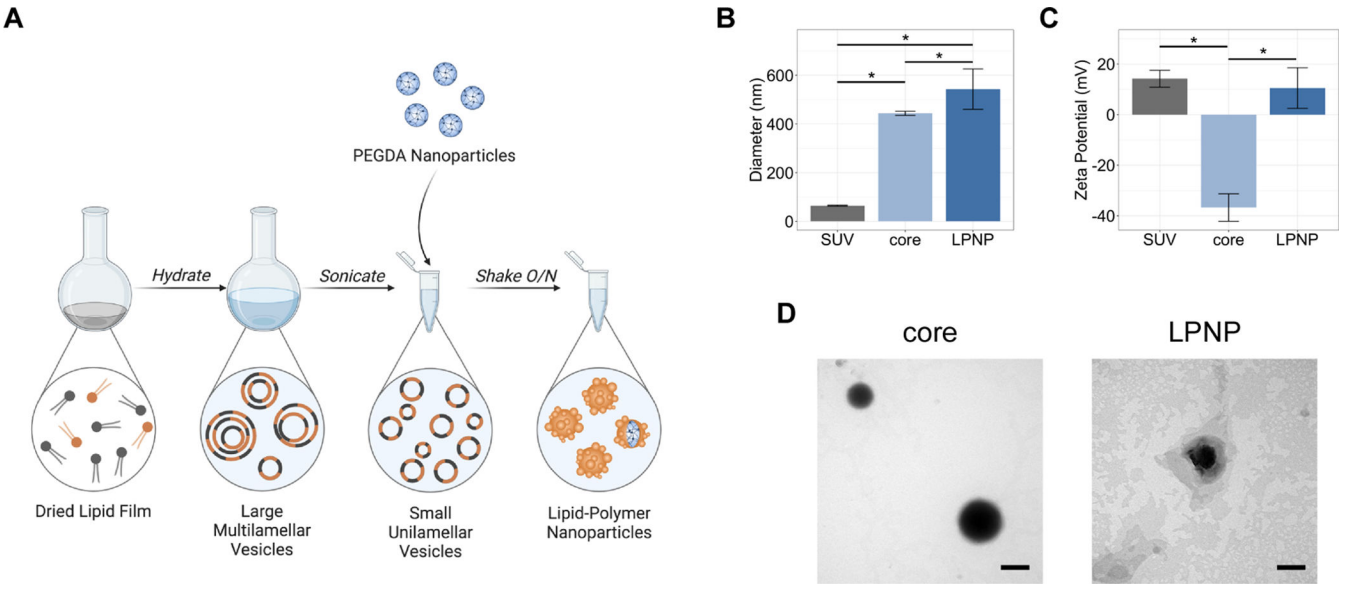

Figure 3.

Coating polymeric cores in liposomes. (A) Schematic of coating cores. SUVs are formed through thin film hydration and sonication. SUVs and polymeric cores are mixed and shaken together overnight to facilitate coating. (B–D) Representative data for coating stiff/large nanoparticles in SUVs with PS. (B) DLS *Z*-average size shows increase in size with coating. (C) ζ-Potential shifts from highly negative toward slightly positive value of SUV. (D) Representative TEM images of nanoparticle cores being coated in SUVs. Darker larger objects are the polymeric cores which are surrounded by the lightly stained SUVs. Scale bar = 200 nm ($n = 5$, $*p < 0.05$, one-way ANOVA).

Author Manuscript Author Manuscript Author Manuscript Author Manuscript

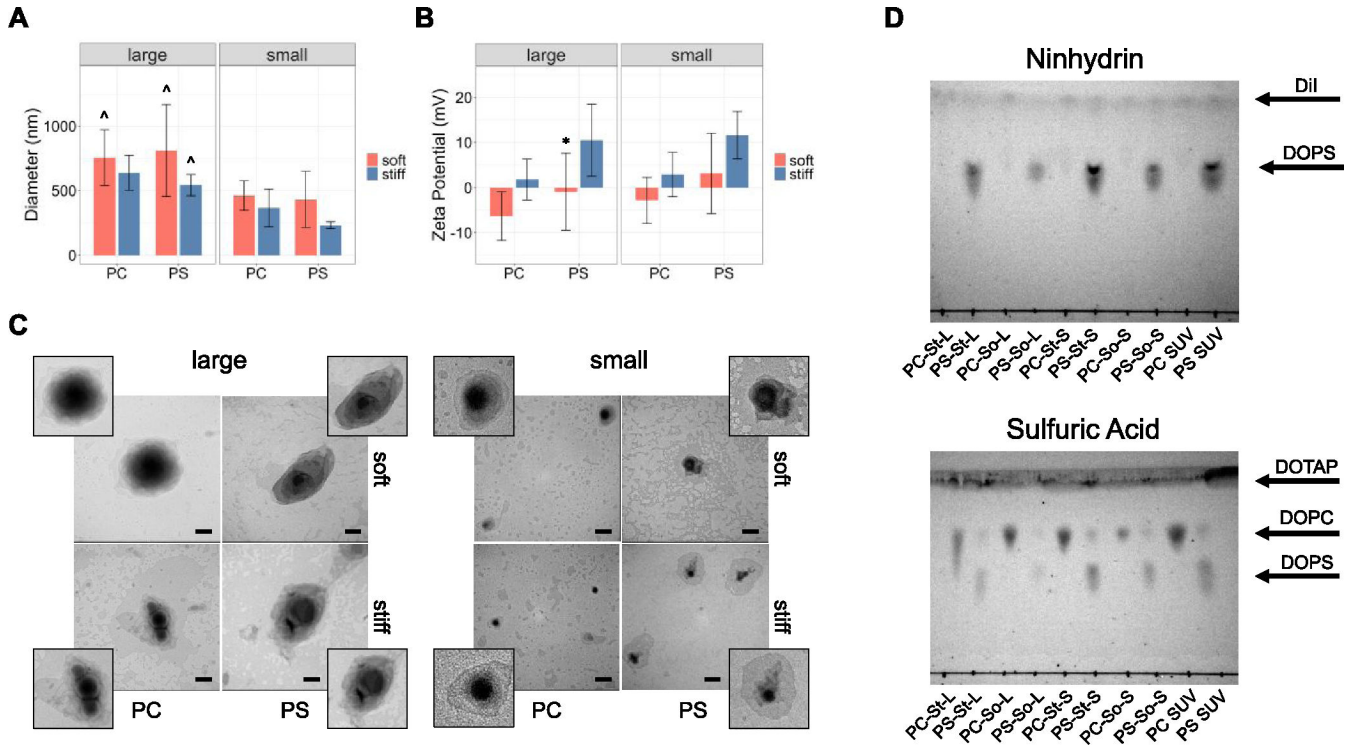

Figure 4.

Characterization of lipid-polymer nanoparticles. (A) Large LPNPs range in diameter from 543 to 812 nm while small LPNPs range in diameter from 232 to 462 nm. PC-St-L is the only large LPNP that is not significantly larger than its small counterpart. There are no significant differences in size within the large or small LPNP groups. (B) ζ-Potential measurements show that all LPNPs are close to neutral, ranging from −6.3 to +11.6 mV. (C) Representative TEM images show a multilamellar structure of lipid surrounding the polymer cores. Additional images can be found in Figures S3 and S4. Scale bar = 200 nm. (D) Thin-layer chromatographs stained with ninhydrin for PS and sulfuric acid for all unsaturated lipids show presence of lipids on all LPNPs ($n = 5$, $p < 0.05$, * compared to matched soft, ^ compared to matched small, three-way ANOVA).

Author Manuscript Author Manuscript Author Manuscript Author Manuscript

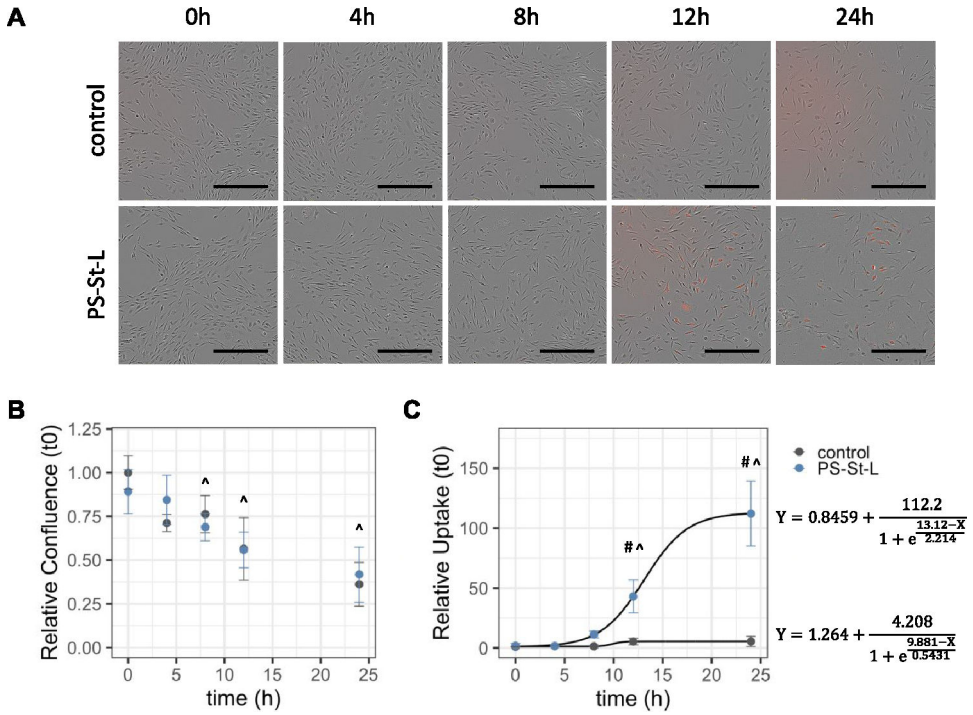

Figure 5.

PS-St-L LPNP uptake was observed over time. (A) Representative images of BMDMs with no LPNPs (control) or PS-St-L LPNPs at 0, 4, 8, 12, and 24 h. Red fluorescence indicates uptake of LPNPs. Scale bar = 200 μm. (B) BMDM confluence over time relative to maximum confluence. Confluence of both control and PS-St-L decrease over time with 8, 12, and 24 h being significantly lower than 0 h. Treatment with PS-St-L LPNPs does not decrease confluence any faster than without. (C) Uptake relative to minimum uptake increases significantly for PS-St-L at 12 and 24 h compared to 0 h. Data is fitted with a Boltzmann sigmoid model ($n = 3$, $p < 0.05$, # compared to control at same time, ^ compared to time = 0 h, two-way ANOVA).

Author Manuscript Author Manuscript Author Manuscript Author Manuscript

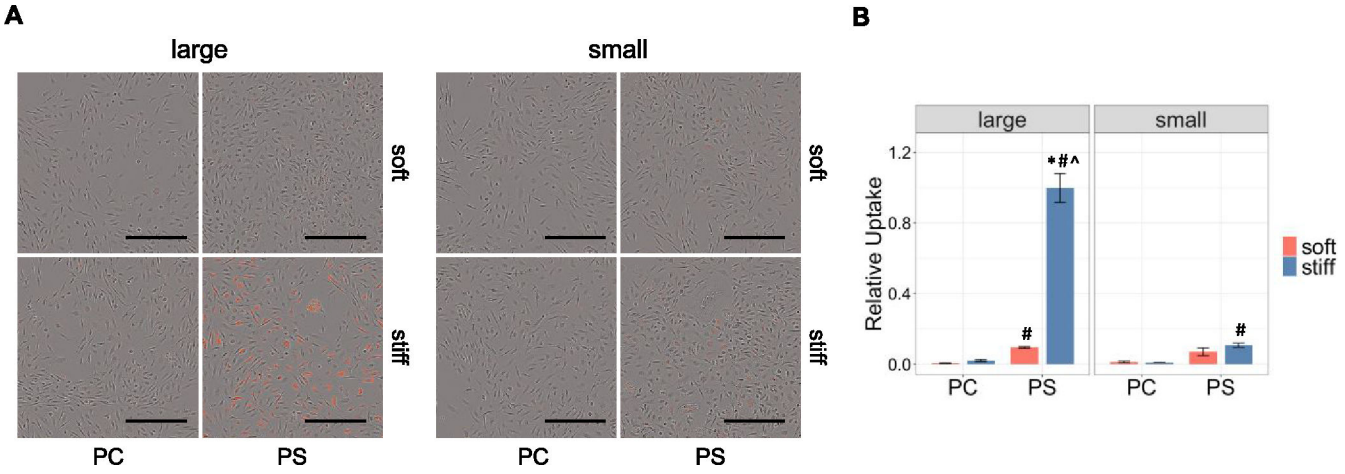

Figure 6.

LPNP uptake by BMDMs after 12 h. (A) Representative images of macrophages with LPNPs. Red fluorescence shows presence of LPNPs within the cells. Scale bar = 200 μm. (B) Fluorescence from images represented in (A) is quantified and normalized to total media fluorescence and maximum uptake. PS-St-L LPNPs are taken up significantly more than any other LPNPs. PS-So-L and PS-St-S LPNPs are also taken up more than their PC counterparts (PC-So-L and PC-St-S, respectively). PS alone is enough to impact uptake; however, stiffness and size play secondary roles in increasing that uptake ($n = 3$, $p < 0.05$, * compared to matched soft, ^ compared to matched small, # compared to matched PC, three-way ANOVA).

Author Manuscript Author Manuscript Author Manuscript Author Manuscript

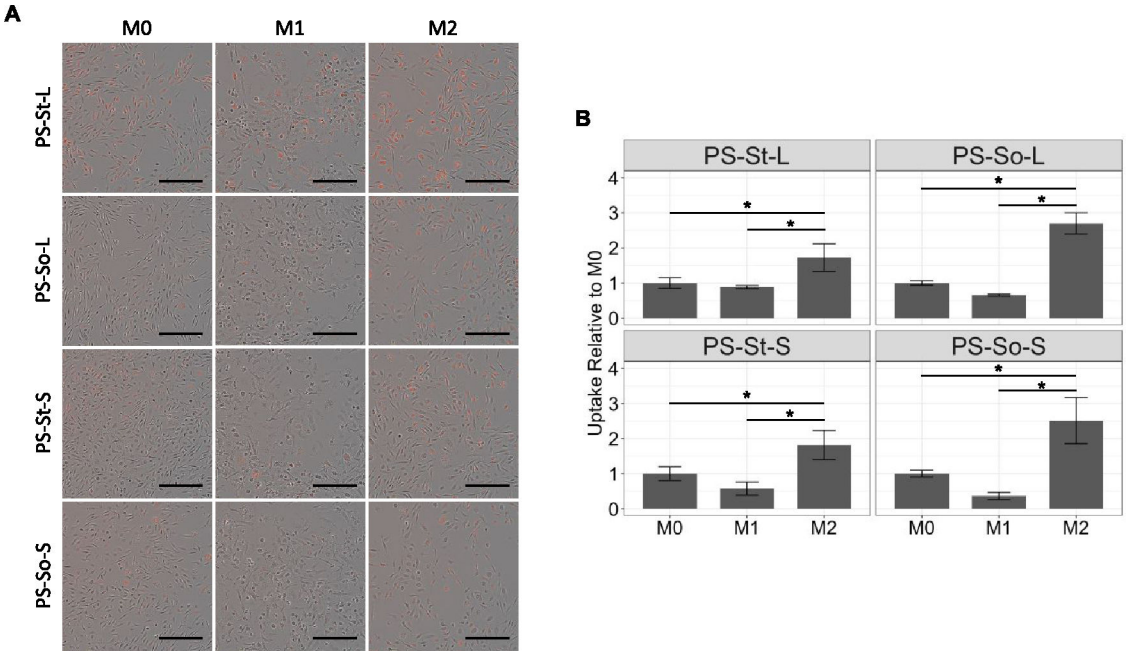

Figure 7.

PS LPNP uptake in polarized macrophages. (A) Representative images of macrophages polarized for 24 h with 50 ng/mL LPS (M1) or 20 ng/mL IL-4 (M2) then given PS LPNPs for 12 h. Scale bar = 200 μm. (B) Uptake relative to uptake in M0 for each LPNP. M2 BMDMs take up more LPNPs than M0 and M1 for all LPNPs tested ($n = 3$, $^*p < 0.05$, one-way ANOVA).

Author Manuscript Author Manuscript Author Manuscript Author Manuscript

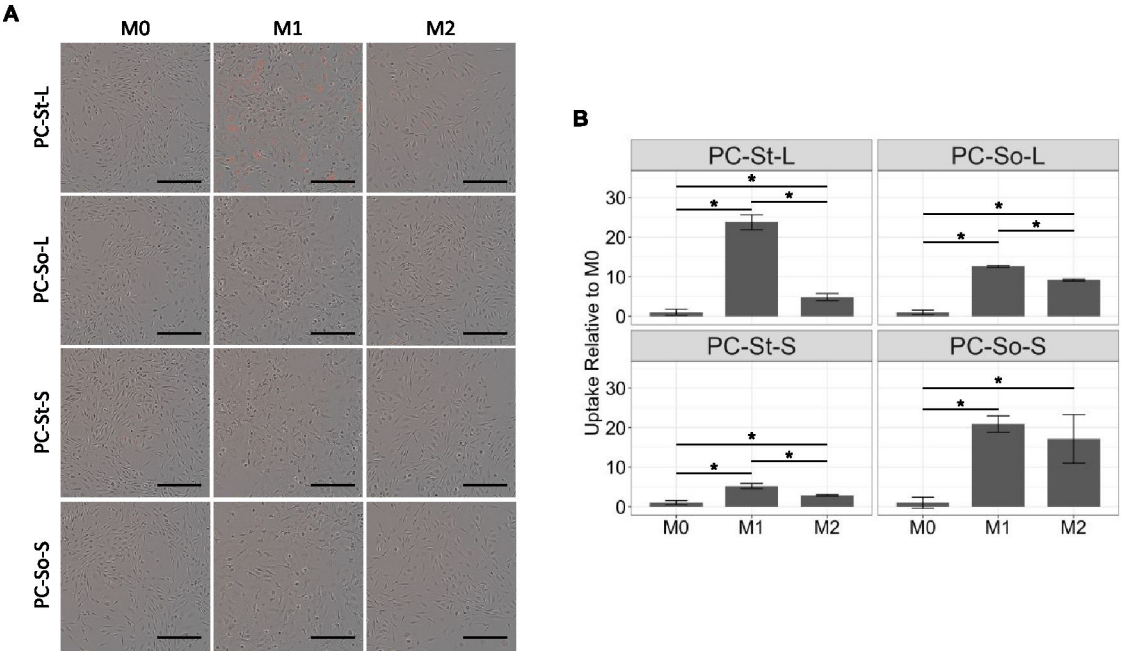

Figure 8.

PC LPNP uptake in polarized macrophages. (A) Representative images of macrophages polarized for 24 h with 50 ng/mL LPS (M1) or 20 ng/mL IL-4 (M2) then given PC LPNPs for 12 h. Scale bar = 200 μm. (B) Uptake relative to uptake in M0 for each LPNP. Polarized BMDMs take up more LPNPs than M0 for all PC LPNPs. M1 BMDMs take up more PC-St-L, PC-So-L, and PC-St-S than M2 ($n = 3$, $^*p < 0.05$, one-way ANOVA).

Author Manuscript Author Manuscript Author Manuscript Author Manuscript

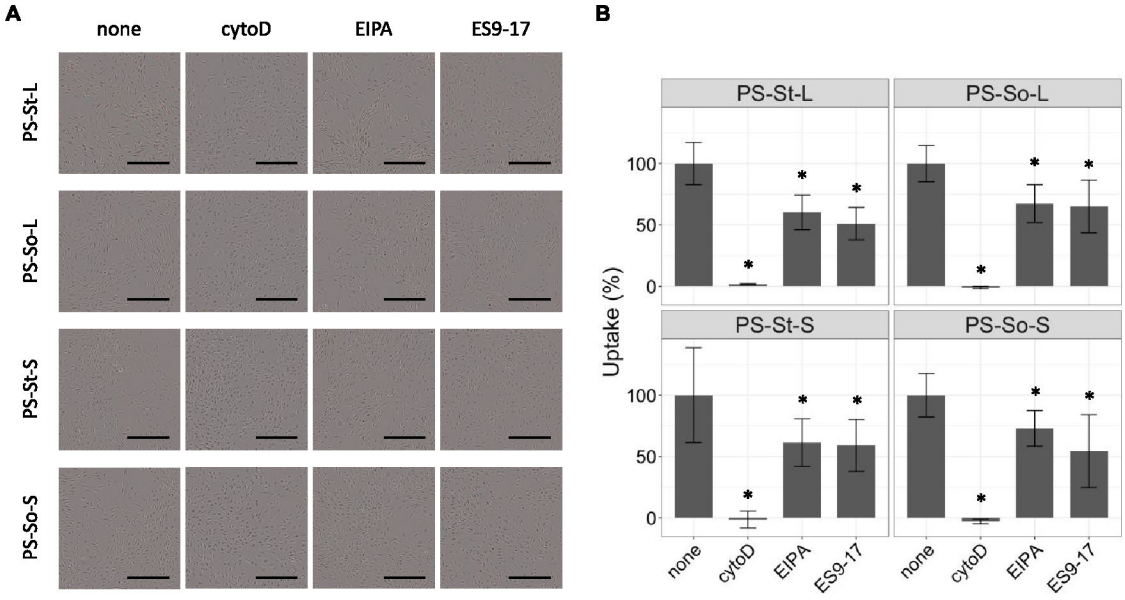

Figure 9.

Endocytosis inhibition at 12 h. (A) Representative images captured by Incucyte S3. Scale bar = 200 μm. (B) Uptake relative to no inhibitor for each PS LPNP. Treatment with cytoD, EIPA, and ES9–17 reduces uptake of all PS LPNPs below 100% ($n = 6$, $^*p < 0.05$ compared to none, two-way ANOVA).

Author Manuscript Author Manuscript Author Manuscript Author Manuscript

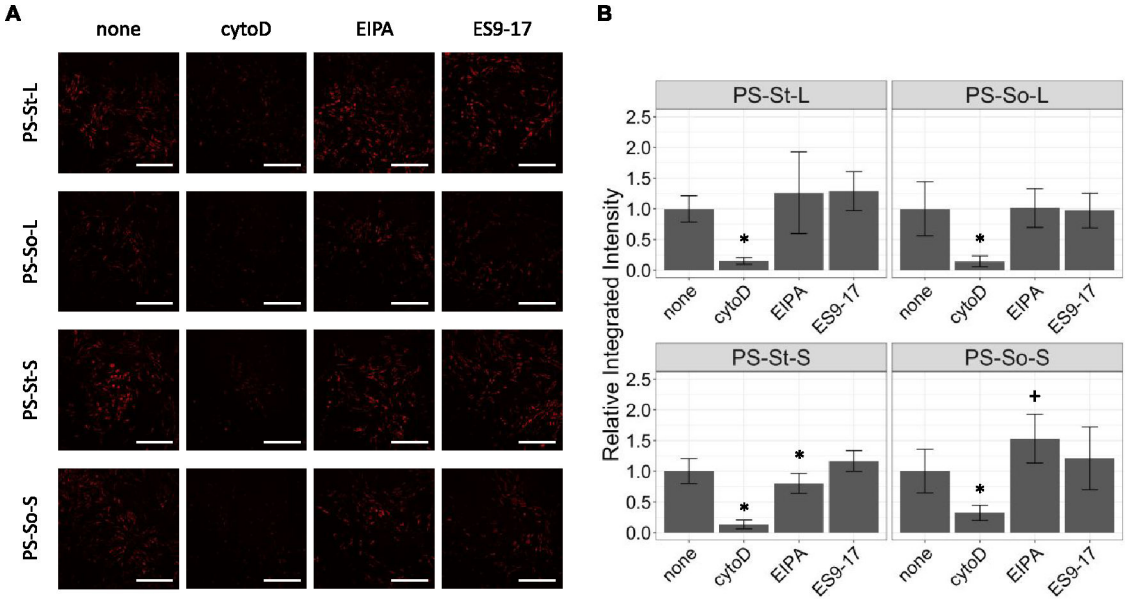

Figure 10.

Endocytosis inhibition at 4 h. (A) Representative images captured by confocal microscope. Scale bar = 200 μm. (B) Integrated red fluorescence intensity relative to no inhibitor. Treatment with cytoD reduces uptake for all PS LPNPs while treatment with EIPA reduces uptake of PS-St-S and increases uptake of PS-So-S. ES9–17 has no effect (n = 10 technical replicates, $p < 0.05$ * reduced from none, + increased from none, one-way ANOVA).

Author Manuscript Author Manuscript Author Manuscript Author Manuscript

Table 1.

Chemical Endocytosis Inhibitors

endocytosis pathway	inhibitor	inhibitor target	concentration range (mM)	concentration selected (mM)
actin-dependent pathways	cytochalasin D	actin polymerization	2.5–20	20
macropinocytosis	5-(*N*-ethyl-*N*-isopropyl)amiloride	Na+/H+ exchange	6.25–50	25
clathrin-mediated endocytosis	ES9–17	clathrin heavy chain	25–200	100

ACS Biomater Sci Eng. Author manuscript; available in PMC 2024 June 24.

Author Manuscript

Author Manuscript

Author Manuscript

Author Manuscript

Table 2.

DLS Values for the PEGDA Cores

	***Z*-average diameter (nm)**	**PdI**
So-L	517.9	0.203
St-L	443.6	0.0429
So-S	206.8	0.112
St-S	152.1	0.0993

Author Manuscript

Author Manuscript

Author Manuscript

Author Manuscript

Table 3.

DLS Values for LPNPs

	***Z*-average diameter (nm)**	**PdI**
PC-So-L	755.8	0.301
PC-St-L	638.3	0.177
PS-So-L	811.9	0.397
PS-St-L	542.8	0.188
PC-So-S	462.3	0.257
PC-St-S	366.0	0.196
PS-So-S	432.8	0.244
PS-St-S	232.3	0.123

Author Manuscript Author Manuscript Author Manuscript Author Manuscript

Table 4.

LPNP Nomenclature[a]

	centrifugation speed fraction	PEGDA (%)	SUV formulation
PC-So-L	5000*g*	10	DPPC/DOPC/DiI
PC-St-L	5000*g*	40	DPPC/DOPC/DiI
PS-So-L	5000*g*	10	DPPC/DOPC/DOTAP/DOPS/DiI
PS-St-L	5000*g*	40	DPPC/DOPC/DOTAP/DOPS/DiI
PC-So-S	20,000*g*	10	DPPC/DOPC/DiI
PC-St-S	20,000*g*	40	DPPC/DOPC/DiI
PS-So-S	20,000*g*	10	DPPC/DOPC/DOTAP/DOPS/DiI
PS-St-S	20,000*g*	40	DPPC/DOPC/DOTAP/DOPS/DiI

[a]So: Soft; St: Stiff; L: Large; S: Small.